

Article

Tribological Properties of Different-Sized Black Phosphorus Nanosheets as Water-Based Lubrication Additives for Steel/Titanium Alloy Wear Contact

Shaowen Dong ^{1,*}, Wei Wang ^{1,*} , Yuan Gao ¹ and Guanyu Deng ^{2,*}

¹ School of Metallurgy Engineering, Xi'an University of Architecture and Technology, Xi'an 710055, China; 15399057390@163.com (S.D.); yuan-gao@xauat.edu.cn (Y.G.)

² School of Mechanical, Materials, Mechatronics and Biomedical Engineering, University of Wollongong, Wollongong, NSW 2522, Australia

* Correspondence: gackmol@163.com (W.W.); gd577@uowmail.edu.au (G.D.)

Abstract: Titanium alloys are extensively used in the aerospace, chemical, and biomedical industries. However, it has always been a challenge in the manufacturing and machining of titanium alloys because they exhibit poor friction and wear characteristics, which results in serious problems and significantly restricts their further production and application. Therefore, in the present study, the wear contact between GCr15 steel and Ti6Al4V alloy is specifically studied by considering black phosphorus nanosheets (BP-NS) as water-based lubrication additives, which is expected to have a great potential application in manufacturing and machining titanium alloys. The influence of BP nanosheet size on the coefficient of friction (COF) and wear rate of Ti6Al4V alloy has been comprehensively studied, based on comparisons among adding large BP nanosheets (L-BP) (2–4 μm), medium BP nanosheets (M-BP) (300–500 nm), and black phosphorus quantum dots (BPQDs) (6–10 nm). Compared with ultrapure water, the COF and wear rate of Ti6Al4V alloy are reduced by 42.4% and 82.3%, respectively, when BPQDs are used as water-based lubrication additives. This paper also shows that a lower COF and wear rate is achieved with the addition of BPQDs than the other two BP nanosheet sizes. Derived from the friction tests and worn surface analysis of Ti6Al4V alloy, lubrication mechanisms of different-sized BP lubricants were proposed. The interlaminar shearing between BP-NS and the adsorbed films were the main mechanisms for L-BP and M-BP lubricants, while the adsorption, repair, and ball-bearing effects were mainly presented in the BPQD lubricants. The discoveries in this paper would be beneficial to developing novel lubricants for the manufacturing and machining of titanium alloys.

Keywords: titanium alloys; manufacturing and machining; black phosphorus; lubrication additives; tribological properties



Citation: Dong, S.; Wang, W.; Gao, Y.; Deng, G. Tribological Properties of Different-Sized Black Phosphorus Nanosheets as Water-Based Lubrication Additives for Steel/Titanium Alloy Wear Contact. *Metals* **2022**, *12*, 288. <https://doi.org/10.3390/met12020288>

Academic Editor: Michael M. Khonsari

Received: 3 January 2022

Accepted: 30 January 2022

Published: 7 February 2022

Publisher's Note: MDPI stays neutral with regard to jurisdictional claims in published maps and institutional affiliations.



Copyright: © 2022 by the authors. Licensee MDPI, Basel, Switzerland. This article is an open access article distributed under the terms and conditions of the Creative Commons Attribution (CC BY) license (<https://creativecommons.org/licenses/by/4.0/>).

1. Introduction

Titanium alloys are extensively used in aerospace, chemical, and military industries due to their high strength, favorable corrosion resistance, and better high-temperature properties [1–4]. Nevertheless, titanium and titanium alloy are a typical difficult-to-cut metal, due to high processing temperature and chemical activity, low deformation coefficient, and elastic modulus during processing, which faults limited further application of titanium alloy in the precision parts of the aviation industry [5–7]. Therefore, it is very important to enhance the workability of titanium and titanium alloys. To solve the problems of titanium alloy machining, adding lubrication additives are often used. In view of the difficulties of titanium alloy processing, traditional metalworking fluids are difficult to lubricate effectively during the processing process of titanium alloy [8–11]. In recent years, water-based lubricants have been broadly applied in the metalworking due to their stable chemical properties, high extreme pressure, anti-wear properties, and good cooling

capacity. Several studies have shown that adding nanomaterials into water is an effectively methods to improve the lubrication properties [12–14].

The special physical and chemical properties of the nanomaterials have attracted widespread attention in lubrication additives fields [15–17]. The nanomaterials dispersed into the lubrication fluid could enter into the frictional area and form the lubrication film on the surface of metals due to their small sizes [18,19]. Black Phosphorus (BP), as an emerging two-dimensional material, is often used in optical, electrical, and mechanical fields [20,21]. At present, in the area of macroscopic and microscopic tribology, the tribological behaviors of BP-NS as lubrication materials have also attracted the attention of researchers. In our previous investigations, compared with traditional two-dimensional materials (Graphene, Molybdenum Disulfide), BP-NS as n-Hexadecane (16C)-based lubrication additives presented excellent wear resistance [22]. Wang et al. used NaOH-modified BP-NS as a lubrication additive and achieved super-lubricity. The reason is that during the sliding process, the BP-OH nanosheets in the silica gel layer formed by hydrolysis reactions, because the water layer is attached to the BP-OH nanosheets through hydrogen bonds, thus obtaining strong super-lubricity [23]. Wu et al. [24] clearly observed that the frictional force at the degradation area of BP-NS was reduced by about 50% with an atomic force microscope. BPQDs, another zero-dimensional nanomaterial of BP, as water-based lubrication additives, could demonstrate tremendous potential due to the uniform size and good water dispersion. The BPQDs prepared by Ren can be stably dispersed in an aqueous solution of glycol, while achieving macroscopic super-lubricity at a contact pressure of 336 mpa (μ , 0.002) [25]. Tang et al. [26] added BPQDs to triethanolamine aqueous solutions, and the results showed that BPQDs lubrication additives exhibited significant anti-friction and anti-wear properties even at ultra-low concentrations (0.005 wt.%). Seminal works have demonstrated that BP-NS and BPQDs have excellent lubrication performance as lubrication additives.

The focus of this research is the tribological properties of different-sized BP-NS as lubrication additives for the GCr15/Ti6Al4V alloy contact. The BP-NS were thoroughly analyzed for morphology, structure and composition using microscopic and spectroscopic techniques. Lubrication mechanisms were discussed and analyzed by tribological tests and wear surface analysis. This study describes the potential novel applications for different-sized BP-NS as water-based lubrication additives.

2. Experimental

2.1. Materials

Red phosphorus (RP) (99.999%, Guangzhou Chemical Reagent Factory, Guangzhou, China), N-methylpyrrolidone (NMP) ($\geq 99.5\%$, Aladdin reagent factory, Shanghai, China), and anhydrous ethanol ($\geq 99.7\%$) were used as raw materials. All reagents did not require further purification unless otherwise stated. Ultrapure water with an electrical resistivity of about 18.25 M Ω ·cm was used.

2.2. Preparation of Different-Sized BP-NS as Lubrication Additives

As shown in Figure 1, different-sized BP-NS as lubrication additives were prepared by high-energy ball milling (HEBM) and sample exfoliation methods. The mass ratio of Gcr15 ball (Φ 10 mm, Φ 6 mm) to red phosphorus, ball milling time, and rotation speed are 50:1, 1 h, and 1000 rpm. The final BP powders were collected and stored in an argon glove box.

The preparation method of L-BP is as follows. The BP powders were dispersed into NMP and sonicated in an ice bath for 8 h. The ultrasonic black solutions were centrifuged at 3500 rpm for 15 min and collected. The obtained precipitates were washed three times using alcohol and ultrapure water. Similarly, the black solutions were centrifuged at 3000 rpm to obtain the supernatant and then centrifuged at 7500 rpm for 25 min to obtained M-BP.

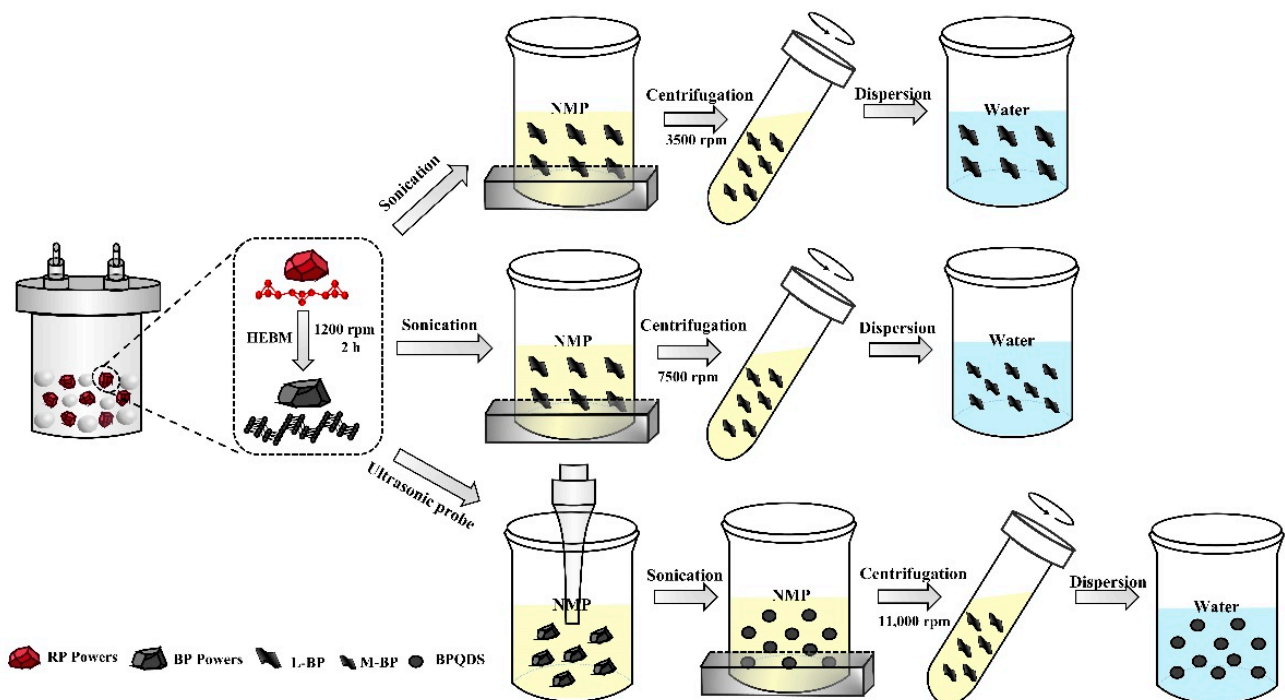


Figure 1. Synthesis process of different-sized BP-NS as lubrication additives.

The preparation method of BPQDs is as follows. The BP powders were dispersed into NMP and sonicated with a probe sonicator for 3 h, followed by ice bath sonication for 8 h. The black solutions were centrifuged at 3500 rpm for 15 min and 7500 rpm for 25 min to obtain the supernatant, and finally centrifuged at 11,000 rpm for 30 min to collect the precipitation. After washing precipitates, the BPQDs were obtained by the vacuum freeze dryer.

The obtained L-BP, M-BP, and BPQDs powder were dispersed into the ultrapure water with the concentrations of 0.025, 0.05, 0.075, and 0.1 wt.% by ultrasonication for 1 h.

2.3. Characterization

The phase structures of L-BP, M-BP, and BPQDs were analyzed by X-ray diffraction (XRD, Bruker D8) (BRUKER, Billerica, USA) and a Raman spectrometer (Raman, Horiba Scientific LabRAM HR Evolution) (HORIBA Scientific, Kyoto, Japan). A scanning electron microscope (SEM, Zeiss Sigma 300) (Zeiss, Oberkochen, German) with an energy dispersive spectrometer (EDS) (Zeiss, Oberkochen, German) were used to observe the micromorphology and size distribution of the BP and RP powders. The microscopic morphologies of BPQDs, L-BP, and M-BP were further characterized by a transmission electron microscope (TEM, FEI Talos F200i) (FEI Company, Hillsboro, OR, USA). The wear surfaces of the steel ball and Ti6Al4V disc were analyzed by SEM and EDS. The wear scar profile and wear volume were measured with the 3D scanning profiler. Finally, the element composition of wear track is examined by Raman scattering and an X-ray photoelectron spectroscopy (XPS, PHI). (ULVAC-PHI, Kyoto, Japan)

2.4. Tribological Tests

The tribological properties of GCr15/Ti6Al4V with ultrapure water and the lubrication additives were studied by ball-on-disc tribo-tester (UMT-5, CETR Corporation) at room temperature. The upper sample is a GCr15 steel ball (Φ 6 mm) and the surface roughness (Ra) is about 18.5 nm. The lower sample is the Ti6Al4V disc (ϕ 24 mm \times 7 mm). The samples were standard samples and the chemical composition is shown in Tables 1 and 2.

Table 1. The chemical composition of the Ti6Al4V disc.

Component	Al	V	Fe	Ti
Percentage (wt.%)	6.59	4.77	0.035	Bal

Table 2. The chemical composition of the Gcr15 ball.

Component	C	Si	Mn	Cr	Fe
Percentage (wt.%)	0.95–1.05	0.15–0.35	0.25–0.4	1.40–1.65	Bal

The tribological tests were performed for 30 min. The radius of rotation, the rotation speed, and the loads were 3.5 mm, 150 r/min, and 8 N–15 N, respectively. All tests were duplicated five times under each condition to confirm the reproducibility of the results. After tests, the ball and disc were cleaned and dried. The wear rate is calculated using this formula:

$$V = \left(\frac{\pi l}{6}\right) \left(\frac{3d^2}{4} + l^2\right) \quad (1)$$

$$l = r - \sqrt{r^2 - \frac{d^2}{4}} \quad (2)$$

$$W = \frac{V}{P \cdot S} \quad (3)$$

where W , V (mm^3), S (m), r (mm), d (mm), l (mm), and P (N) represent the wear rate, wear volume, sliding distance, ball radius (3 mm), wear diameter, wear height, and load of the balls, respectively. The wear diameter is measured by SEM.

3. Results and Discussion

3.1. Characterization and Analysis of the Initial BP Powders

XRD patterns of RP and BP powders are shown in Figure 2a. The RP powders have two characteristic peaks at $2\theta = 30$ and 55° , corresponding to the amorphous RP. After HEBM for 2 h, two broad characteristic peaks were changed into $2\theta = 26.5^\circ$ (020), 35.0° (021), and 56.0° (111) diffraction peaks, indicating that the BP powder has a standard orthogonal structure (JCPDS Card NO.76-1957) and RP has been converted to BP by HEBM process. In addition, the results of Raman spectroscopy proved the transfer of RP to BP powder (Figure 2b). After the 2 h HEBM process, the characteristic peak of RP at 305 cm^{-1} disappeared and three sharp characteristic peaks appeared in BP, corresponding to the A_g^1 , B_g^2 , and A_g^2 vibrational modes. Figure 2c reflects that the size of the prepared BP powder is between 200 nm and 3 μm . According to EDS analysis, the mass ratio of P is 95.96 wt.% and the mass ratio of O is 4.04 wt.%; moreover, it can be seen from the EDS analysis that the brown image has a lot of P element content, while the oxygen element content is less, indicating that the prepared black phosphorus has a lower degree of oxidation.

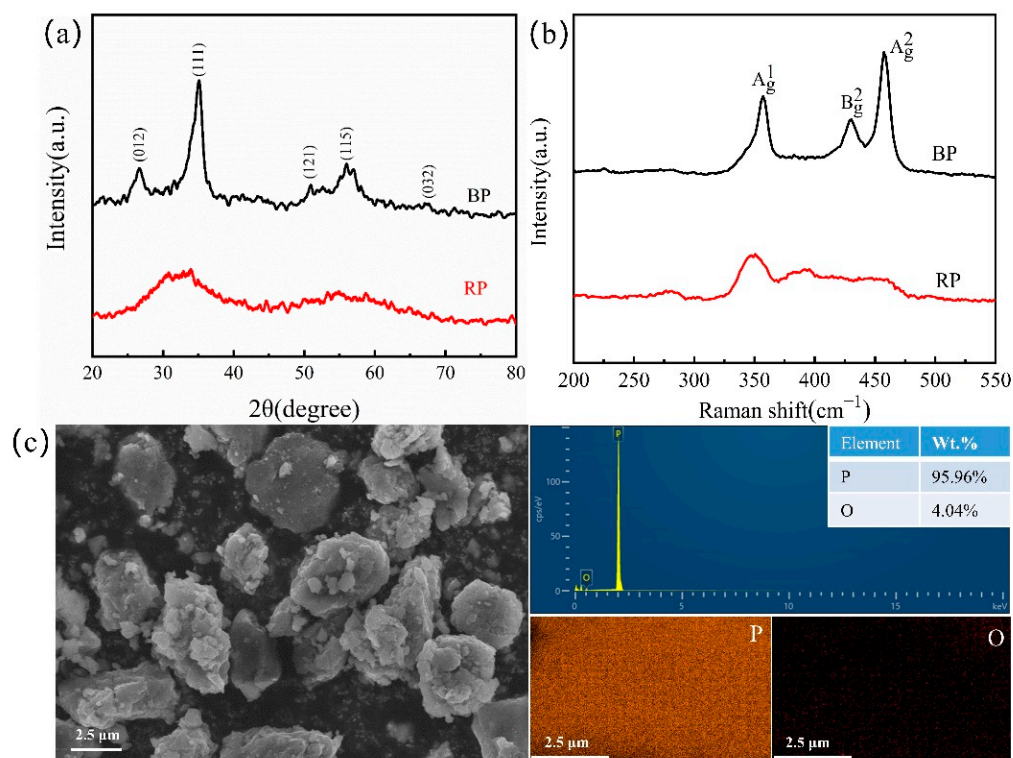


Figure 2. (a) XRD and (b) Raman patterns of RP and BP. (c) SEM image and EDS of BP powders.

3.2. Characterization of Different-Sized BP-NS

The characteristics of L-BP, M-BP, and BPQDs are shown in Figure 3, which indicated that XRD patterns of different-sized BP-NS correspond to the characteristic peaks of the BP powders, and these results are similar to BP orthorhombic crystals (JCPDS No. 74-1878). The diffractive peaks of the L-BP, M-BP, and BPQDs are clearer than that of the BP powders. The blue shift occurred on the (111) plane, indicating that different-sized BP-NS have better crystallinity. The figure of the Raman spectrum (Figure 3c) reveals that the diffractive peaks correspond well to the characteristic peaks of A_{1g} , B_{2g} , and A_{2g} in the BP powders. Compared with the diffractive peaks of the BP powders, the diffractive peaks of L-BP, M-BP, and BPQDs have a significant blue shift due to mini-size and functional groups. Especially for the BPQDs samples, the characteristic peaks of A_{1g} , B_{2g} and A_{2g} are blue-shifted by 1.9, 3.4, and 2.1 cm^{-1} , respectively.

To further analyze the chemical composition and states of the different-sized BP-NS, FTIR spectroscopic were performed. As shown in Figure 3d, the characteristic peaks of 2908, 1637, 1153, and 1002 cm^{-1} of different-sized BP-NS can ascribe the stretching vibrations of -OH, C=O, P=O, and P-O. The above peaks are the absorption of H_2O , CO_2 , and the surface oxidation of BP samples. Due to the smaller volume and the larger volume of functional groups of BPQDs, the intensity of the peaks of -OH and C=O in the spectra of BPQDs are much sharper than that in the spectra of L-BP and M-BP. The abundant oxygen-containing groups give the BPQDs good dispersion stability in water.

In order to further analyze the phase structures and morphologies of different-sized BP-NS, transmission electron microscopy (TEM) was adopted (Figure 4). As shown in Figure 4, different-sized BP-NS, with sizes of about 2–4 μm (L-BP), 300–500 nm (M-BP), and 6–10 nm (BPQDs), were successfully prepared. Figure 4c,f,i reflects the HR-TEM images and SAED patterns of different-sized BP-NS. The lattice spacing of L-BP and M-BP is about 0.254 nm, corresponding to the (111) plane of BP. The lattice spacing of BPQDs is about 0.21 nm, corresponding to the (020) plane of BP. From the SAED patterns, it means that the different-sized BP-NS have well-defined diffraction rings, which clearly reflects the good crystallinity of the different-sized BP-NS.

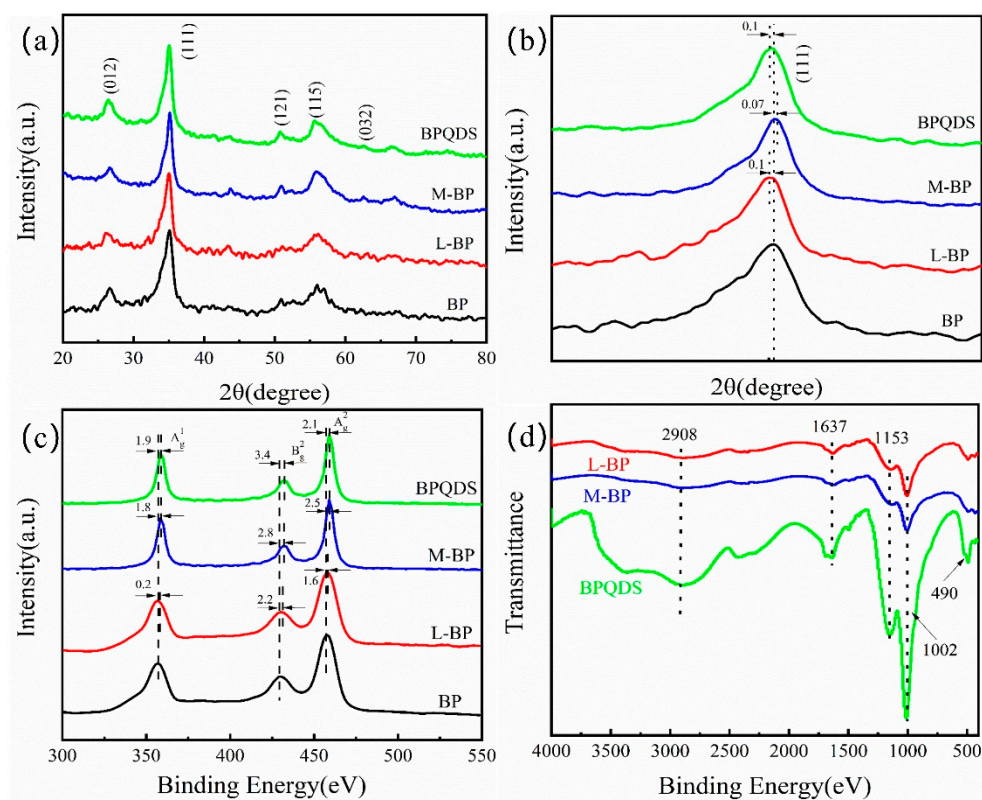


Figure 3. (a) XRD patterns, (b) the partial magnification of the (111) peak, (c) Raman spectrum, and (d) FTIR spectra of different-sized BP-NS.

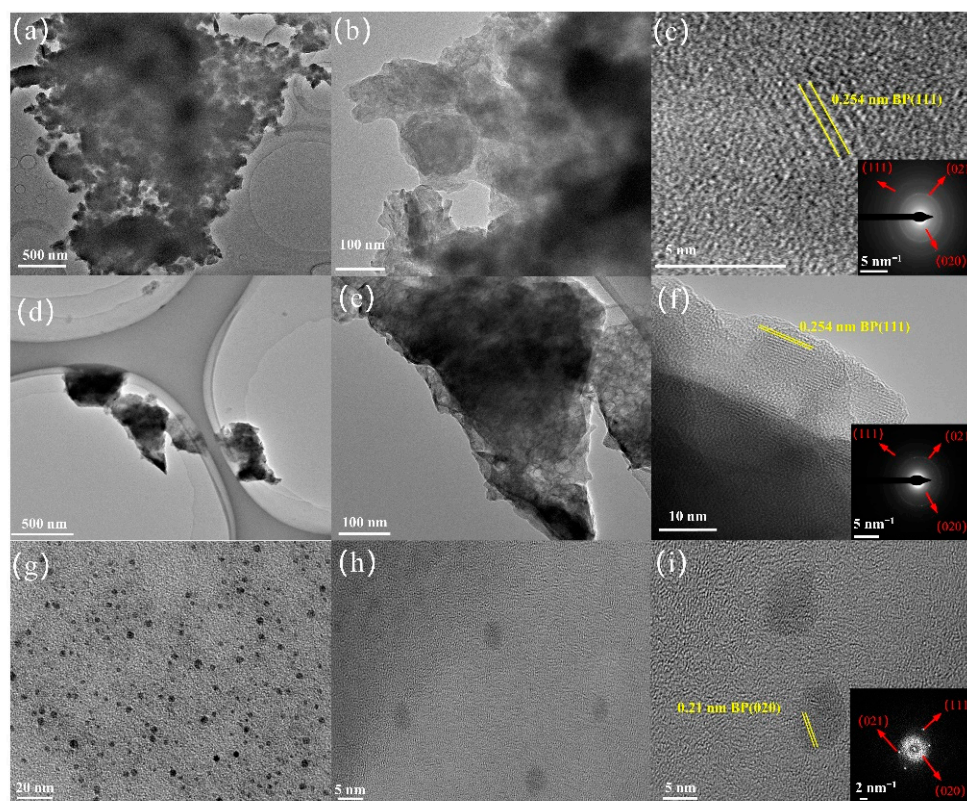


Figure 4. TEM images of the L-BP (a–c), M-BP (d–f), and BPQDs (g–i).

3.3. Tribological Performances

Figure 5a shows the COFs of ultrapure water and different-sized BP-NS as water-based lubrication additives. Compared with ultrapure water, the COFs of lubricants of different-sized BP-NS showed different degrees of reduction. Obviously, the COFs of 0.075 wt.% BPQD lubricants were more stable. The COFs of ultrapure water were firstly increased and then fluctuated over time. The average COF of ultrapure water is about 0.3252. At the time of 17 min, the COF of pure water was increased rapidly until the end of the frictional test. The reason is that during friction and wear, the water film was broken. It leads to the increase of the COF. After adding L-BP and M-BP into ultrapure water, the initial COFs were dropped rapidly and then remained at a stable value. When the small-sized BPQDs is added, in the initial stage, the COFs were lower and stable, indicating that the small-sized BPQDs could quickly enter the friction area and maintain stability. Figure 5b reflects the average COFs and wear rates of ultrapure water and lubricants of different-sized BP-NS. Obviously, L-BP, M-BP, and BPQDs are effective lubrication additives to reduce friction and wear. Compared with ultrapure water, adding 0.075 wt.% BPQDs lubrication additive could reduce COFs from 0.3252 to 0.1870, and the wear rates were decreased from $5.83 \times 10^{-6} \text{ mm}^3$ to $1.03 \times 10^{-6} \text{ mm}^3 (\text{Nm})^{-1}$. The results show that the small-sized BPQDs present excellent wear resistance and can greatly decreased the COF and wear rate.

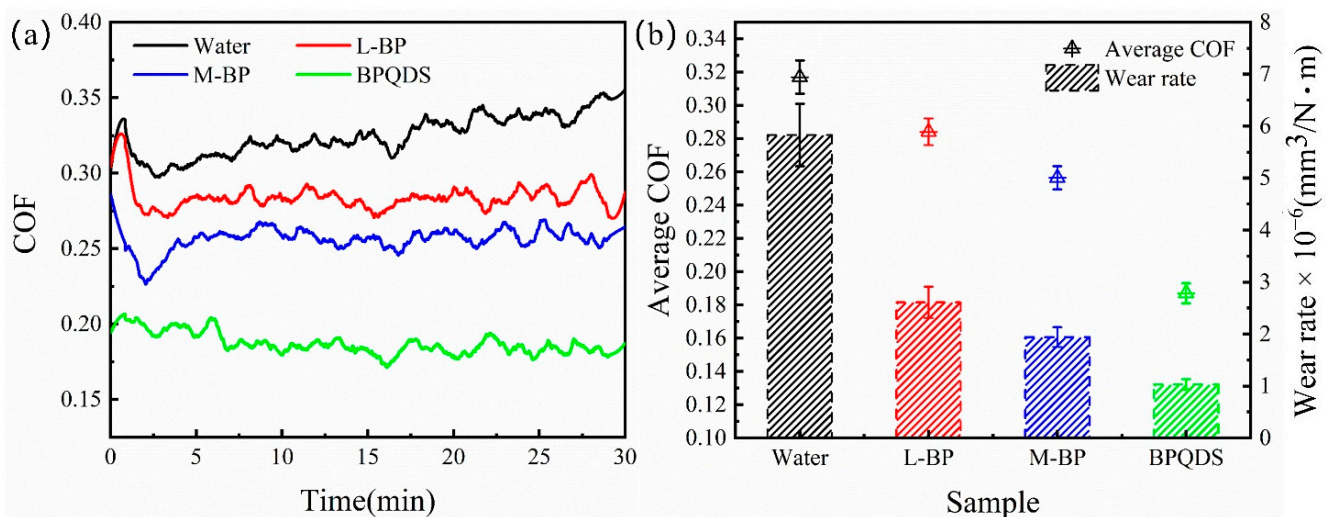


Figure 5. (a) COF versus sliding time. (b) Average COF and wear rate for the ultrapure water and different-sized BP-NS lubricants (0.075 wt.%, 10 N).

The concentration of the lubrication additives has great effect on their lubrication performance; therefore, the effects of the concentrations of the nano-additives on tribological properties were investigated. The COFs and wear rates of different concentrations of BPQD lubricants at the load of 10 N were reflected in Figure 6. As the BPQDs concentration increased, the changes of COF and wear rate show a trend of first decreasing and then increasing. As the concentration of BPQDs lubricating additive increased from 0.00 wt.% to 0.075 wt.%, the COF and wear rate decreased rapidly. The concentration of BPQDs lubricating additive increased from 0.075 to 0.1 wt.%, which may be due to the high concentration of BPQDs, which leads to particle aggregation, thus increasing the COFs and wear rates [27–30].

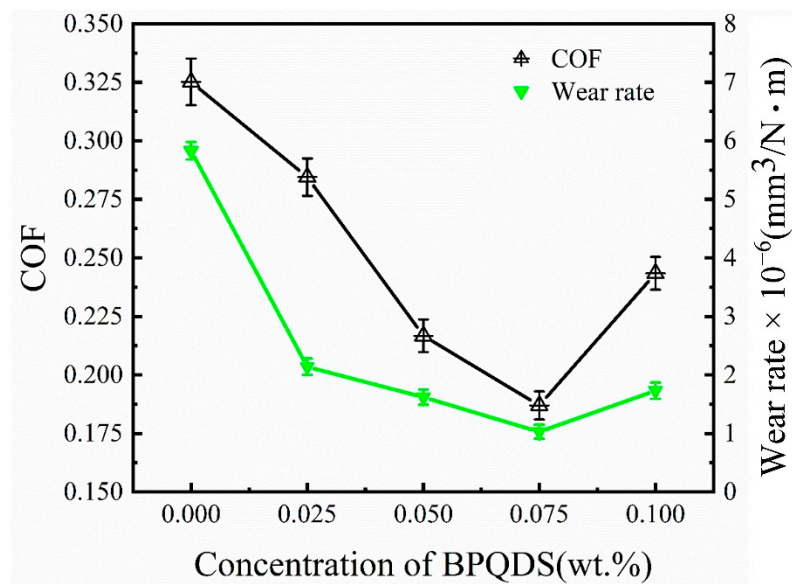


Figure 6. Average COFs and wear rates as a function of BPQDs concentration as water-based lubrication additives (10 N, 150 r/min, 0.5 h).

The tribological properties of different-sized BP-NS under different loads were investigated, as shown in Figure 7a. For ultrapure water, the COFs of L-BP and M-BP were decreased with increasing load. When the loads were increased from 10 N to 15 N, the average COFs of BPQDs increased slightly, although they were still lower than that of other lubrication additives. The reason is that because BPQDs lubrication additives achieve optimal tribological properties at 10 N, when the load increases, the wear rate and friction coefficient increase, which shows that BPQDs lubrication additives are in a boundary lubrication state at high load bearing, resulting in high friction and wear. Figure 7b shows the wear rates of different-sized BP-NS as water-based lubrication additives with different loads. It is not hard to see that the trend of change of wear rates closely resembled COFs'. Combined with the characteristics of COFs (Figure 5a) of different lubrication additives, it means that the short running-in time could lead to lower wear rates. In contrast, the wear rate is high due to the initial instability of the COFs during the friction process. The survey reflected that adding BP-NS into ultrapure water can reduce COF and wear rate. The BPQDs with small sizes have the best tribological properties.

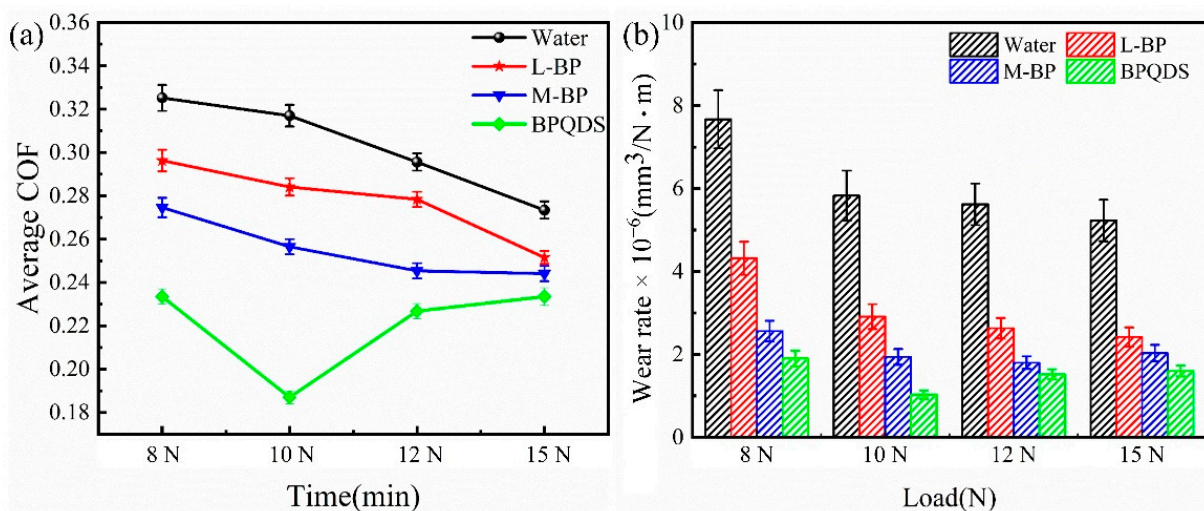


Figure 7. Tribological properties of different lubrication additives with different loads: (a) average COF, (b) wear rate (0.075 wt.%, 150 r/min, 0.5 h).

3.4. Worn Surface Analysis

The wear scar and wear spots lubricated by ultrapure water and lubricants of different-sized BP-NS are reflected in SEM (Figure 8). From the Figure 8a–d, it reflects that the ground spots are oval on the surface of the GCr15 ball. This can be explained that elliptical spots will be formed due to the differential hardness between the ball and the disc [31]. For ultrapure water and different-sized BP-NS, ultrapure water has the widest wear scar of 949 μm . Figure 8(a₂) shows that there are pits on the surface of the disc. After adding L-BP lubrication additives, the wear scar becomes shallower and the wear area becomes smaller. The serious furrow phenomenon was also happened. After adding M-BP lubrication additives, the width of the wear scar became narrower and the wear area became smaller, indicating that the M-BP exhibits better tribological properties at a load of 10 N. In sharp contrast, the scratches of the BPQD lubricants were observed to be the shallowest. Due to the small size effect, BPQDs are more likely to enter the friction contact area and undergo tribological chemical reactions, thereby reducing wear. The survey reflects that the smaller the nanosheets sizes can be obtained, the better tribological properties can be demonstrated.

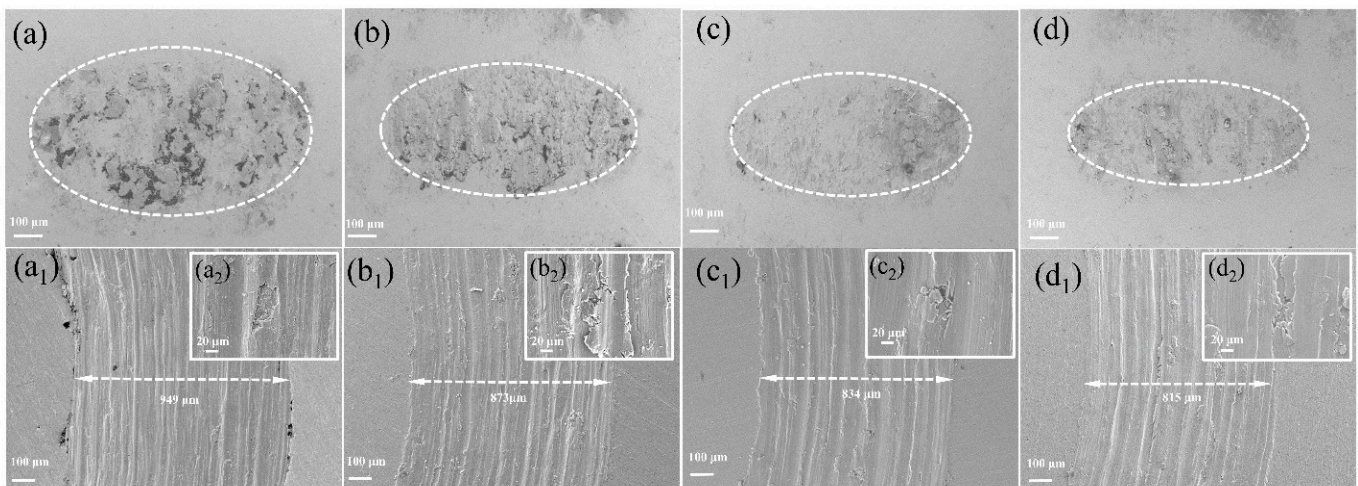


Figure 8. SEM images of worn surface of steel balls and the Ti6Al4V disc lubricated by ultrapure water (a,a₁,a₂), L-BP (b,b₁,b₂), M-BP (c,c₁,c₂), and BPQDs (d,d₁,d₂) (10 N, 150 rpm, 0.075 wt.%).

The EDS spectra of worn surface of Ti6Al4V disc lubricated by ultrapure water and lubricants of different-sized BP-NS are shown in Figure 9. The uniform distributions of Ti and Fe were presented on the wear scar obtained by ultrapure water. Besides these elements, the P element was found at the location of wear scars obtained by L-BP, M-BP, and BPQD lubricants, which means that the adsorption film was formed on the surface of the Ti6Al4V disc. It can be seen from the element content that when using BPQD lubricant, the P content on the surface of Ti6Al4V is up to 0.67 wt.%. This further illustrates that BPQDs can effectively enter the friction contact area to prevent direct contact between the upper and lower samples, thereby reducing friction and wear.

Figure 10 shows a 3D image depth map of the surface wear scars of a Ti6Al4V disc using different lubrication additives. As shown in Figure 10a, the maximum wear amount of ultrapure water is 0.467 mm³, and the wear is relatively large, indicating that the lubrication ability of pure water is poor and corrosion wear occurs during friction. As can be seen from Figure 10b, when using L-BP lubricants, the depth of the wear scar is uneven, indicating the creation of deep grooves, resulting in an increase in wear. Using the M-BP lubricant in Figure 10c, the condition improved slightly, with flat wear scars and less wear. In contrast, using BPQD lubricants, the wear scars of the Ti6Al4V disc have the shallowest wear scars and the narrowest width, with a minimum wear volume of 0.233 mm³ (Figure 10d).

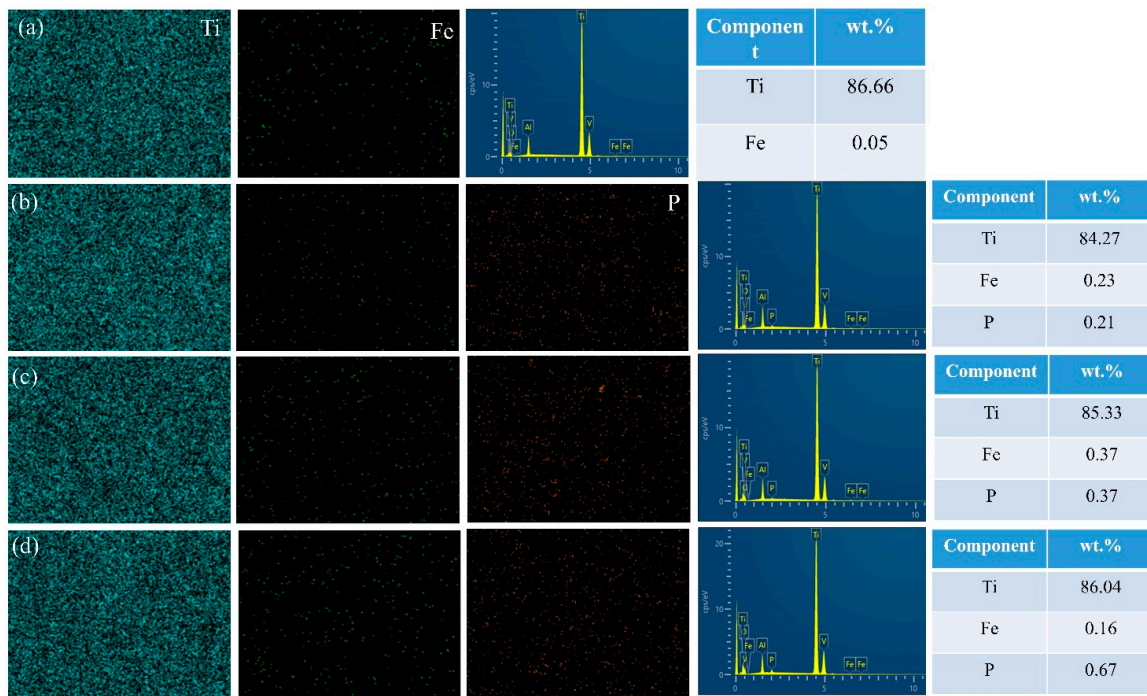


Figure 9. The EDS spectra of the worn surface of Ti6Al4V discs lubricated by (a) Ultrapure Water, (b) L-BP, (c) M-BP, and (d) BPQD lubricant.

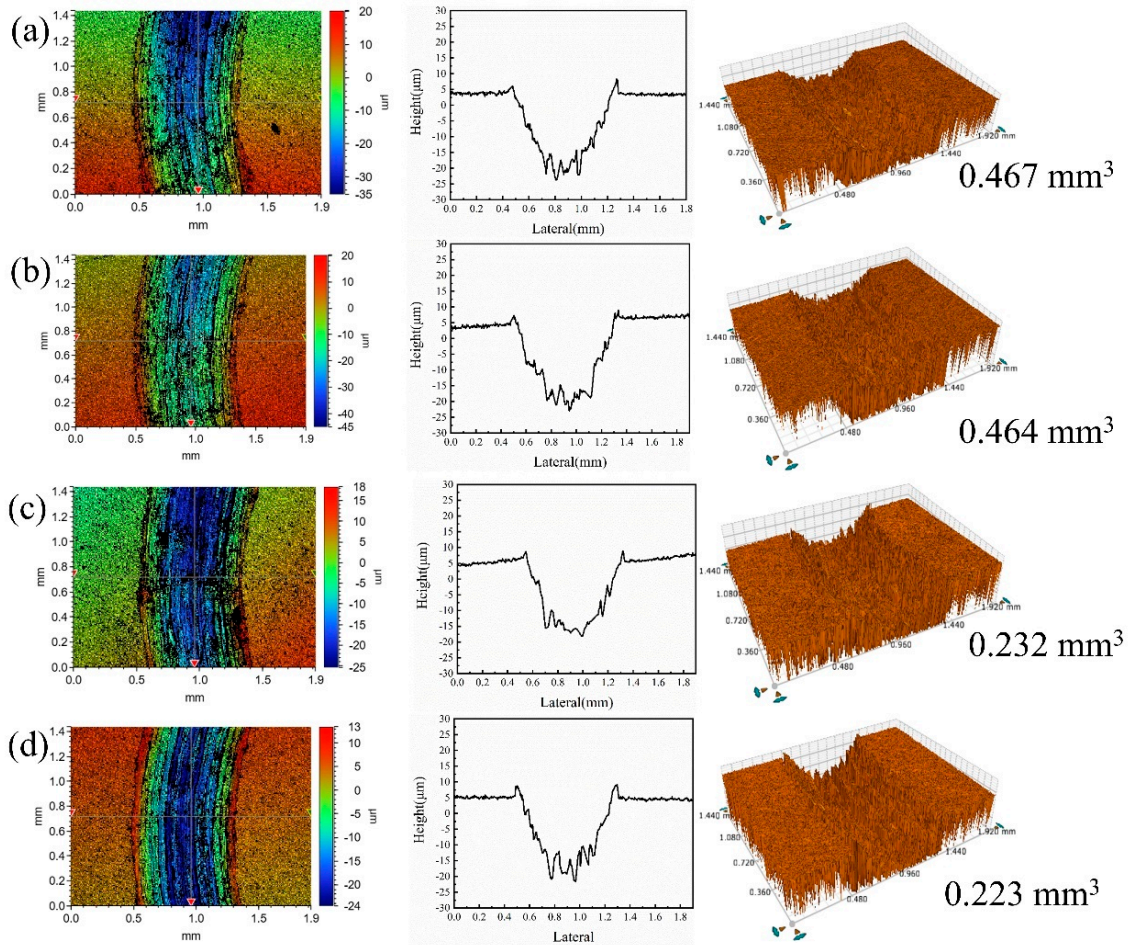


Figure 10. 3D depth maps of the wear scars on the discs lubricated by (a) ultrapure water (b) 0.75 wt.% L-BP, (c) 0.075 wt.% M-BP, and (d) 0.075 wt.% BPQDs (10 N, 150 r/min).

3.5. Lubrication Mechanism of the Lubrication Additives

In order to obtain the lubrication mechanisms of the different-sized BP-NS lubricants, Raman and XPS analysis was adopted. From the Raman spectra of Figure 11(a₁–c₁), the presence of L-BP, M-BP, and BPQDs has been confirmed by the characteristic peaks around 360 cm⁻¹, 430 cm⁻¹, and 460 cm⁻¹ [32]. The survey indicates that an adsorption film is formed on the surface of Ti6Al4V, which has a protective effect on its surface. From Figure 11(a₃–c₃), it can indicate that the application of different lubricants produced TiO₂ and Al₂O₃, as can be perceived from the O1s peaks at 530.2 eV and 532.38 eV [33–35]. Additionally, from Figure 11(a₄–c₄), it can be seen that phosphorus oxides are produced on the friction surface [36]. However, when using BPQDs' lubrication additive, in addition to the above peaks, the GCr15 balls was oxidized to Fe₂O₃, which can be proved by the peak of 531.07 eV in the O1s spectrum in Figure 11(c₃) [37]. Additionally, in Figure 11(c₄), in addition to phosphorus oxides (133.38 eV), the 131.18 eV peak is derived from phosphate [26,36]. It can be inferred that the BPQDs lubrication additive have tribo-chemical reaction on the surface of Ti6Al4V disc and formed a tribo-chemical reaction film consisting of Fe₂O₃, Al₂O₃, TiO₂, phosphorus oxides, and phosphate on the wear surface.

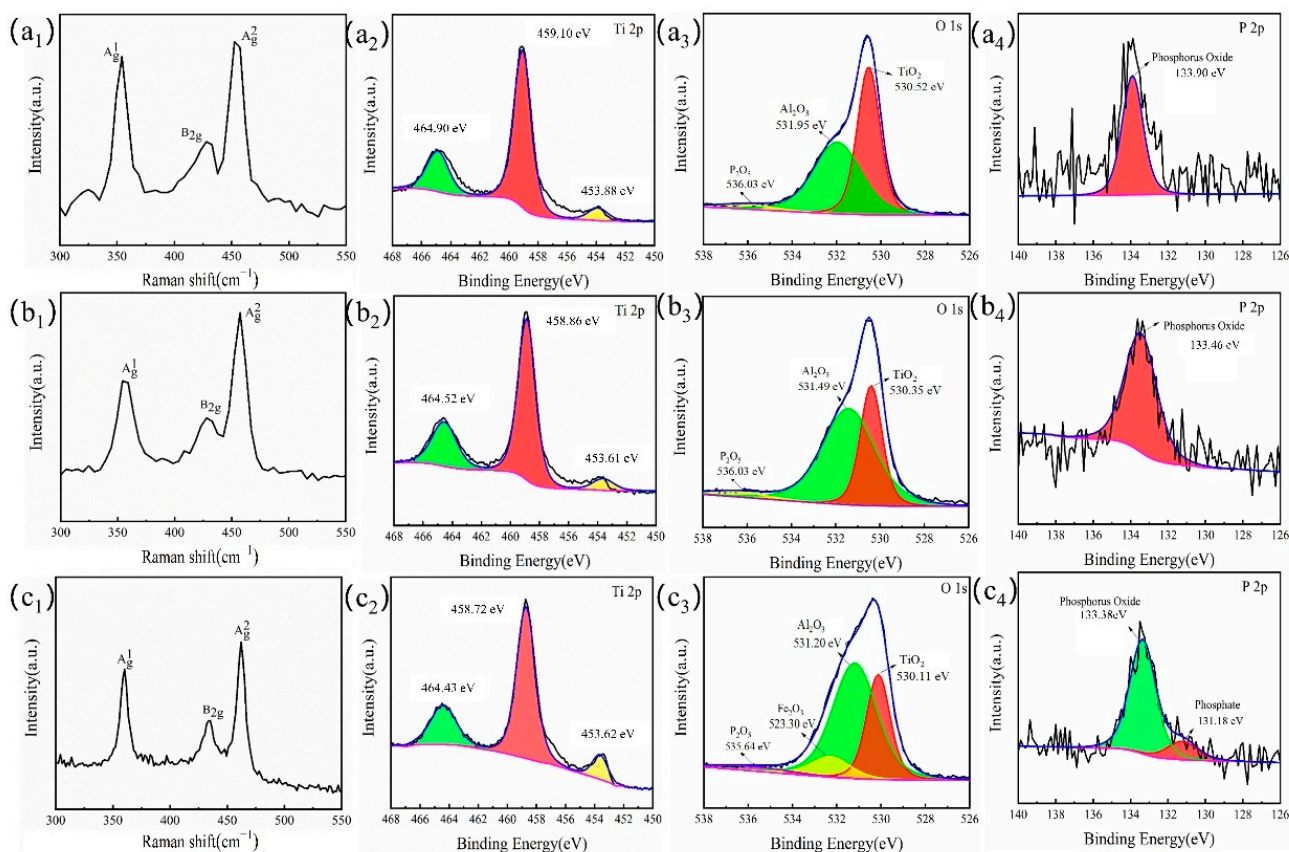


Figure 11. Raman and XPS of the wear scar surface lubricated by the 0.075 wt.% L-BP (a₁–a₄), M-BP (b₁–b₄), and BPQDs (c₁–c₄) lubrication additives (10 N, 150 r/min, 30 min).

The ratio of the film thickness (h_{\min}) to the surface roughness (R_q) of the lubricated surface is used to determine the lubrication state of the frictional process, calculated as follows [38,39]:

$$\lambda = \frac{h_{\min}}{R_q} \quad (4)$$

$$h_{\min} = 2.8R' \left(\frac{\eta\mu_e}{E'R'} \right)^{0.65} \left(\frac{W_y}{E'R'^2} \right)^{-0.21} \quad (5)$$

$$R_q = \sqrt{R_{ball}^2 + R_{disc}^2} \quad (6)$$

where W_y and μ_e are the load (10 N) and sliding speed (64 mm/s), respectively, E' represents the modulus of elasticity (162 GPa), and R' represents the radius of ball (3 mm). Using the equation, the h_{min} is 7.6 nm. The calculated value of the λ is 0.166, which is less than 1, which explains that the lubrication condition is boundary lubrication. The tribological properties of the boundary lubrication are the interaction between the lubricant and the friction surface and the characteristic of the generating boundary lubrication film [40]. Therefore, the addition of lubricating additives into ultrapure water is an effective method to improve lubrication in metalworking.

By analyzing on the results of the surface of the wear scar, the lubrication mechanisms of the different-sized of BP-NS lubricants are proposed (Figure 12). According to XPS and Raman results, the tribological layers including the adsorption film of black phosphorus and the tribo-chemical film were produced on the surface of a Ti6Al4V titanium alloy during the friction process. The lubrication mechanism of L-BP and M-BP is due to the shearing effect between the BP nanosheets to prevent the direct contact of the frictional pairs. The good lubricity of BPQDs is due to its small size for easily accessing to the contact area. The chemical reaction films consisting of Fe_2O_3 , Al_2O_3 , TiO_2 , phosphorus oxides, and phosphates are beneficial to improving lubrication properties. The formed tribological layers can greatly prevent the contact of the friction surface [41–43]. In addition, BPQDs can also be used as the ball bearing in the friction process to decrease friction and wear [44,45]. In conclusion, the reason for the excellent friction performance of BPQD lubricant is that the small size of BPQDs is more likely to enter the contact area to produce an effective tribo-chemical film on the surface of the friction pairs.

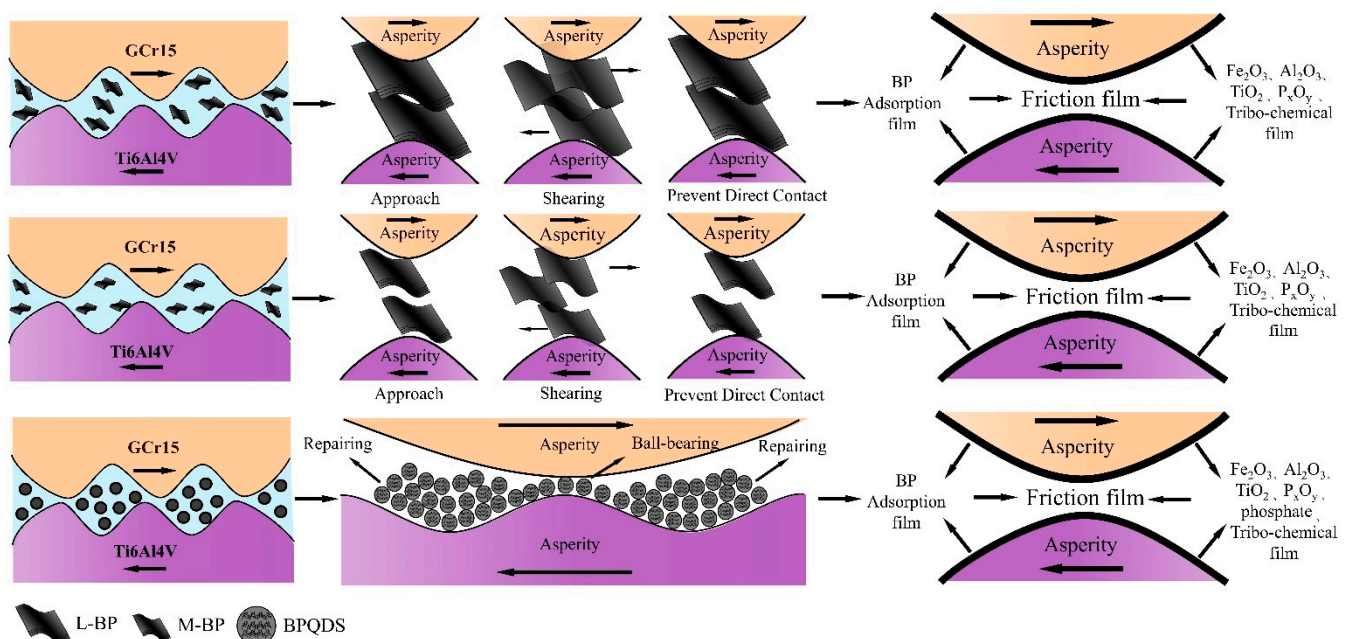


Figure 12. Schematic of lubrication mechanism of L-BP, M-BP, and BPQD lubricants.

4. Conclusions

In general, the different-sized of BP-NS are prepared by HEBM and liquid phase exfoliation methods. The tribological properties of the different-sized of BP-NS as water-based lubrication additives are evaluated under different loads for GCr15/Ti6Al4V contact. The results show that the COFs and wear rates of the different-sized of BP-NS lubricants are decreased to different degrees. The 0.075 wt.% BPQD lubricant exhibits the best tribological properties. Compared with ultrapure water, the COF and wear rate are reduced by about 42.4% and 82.3%, respectively. The lubrication mechanisms can ascribe to the BP adsorption

film and the tribo-chemical film. On the one hand, BPQDs are more likely to enter the contact area. On the other hand, the anti-wear performance of Ti6Al4V depends on the adsorption film and tribo-chemical reaction film. These aspects prevent direct contact on the friction pairs, and effectively improve anti-friction and anti-wear, showing the excellent tribological performance of BPQDs.

Author Contributions: Methodology, W.W.; validation, S.D. and W.W.; investigation, Y.G.; writing—original draft preparation, S.D.; writing—review and editing, S.D., W.W. and G.D. All authors have read and agreed to the published version of the manuscript.

Funding: This work was supported by the fund of the Youth Science and Technology New Star Project of Shaanxi Province Innovation Ability Support Plan (2021KJXX-32) and Advanced technology research program of Xi'an (21XJZZ0031).

Institutional Review Board Statement: Not applicable.

Informed Consent Statement: Written informed consent has been obtained from the patient(s) to publish this paper.

Data Availability Statement: All the original data and graphic files of this study are stored in Figshare. And the DOI number is [10.6084/m9.figshare.19102403].

Conflicts of Interest: The authors declare no conflict of interest.

References

1. Chong, Y.; Deng, G.; Gao, S.; Yi, J.; Shibata, A.; Tsuji, N. Yielding nature and Hall-Petch relationships in Ti-6Al-4V alloy with fully equiaxed and bimodal microstructures. *Scr. Mater.* **2019**, *172*, 77–82. [[CrossRef](#)]
2. Deng, G.; Zhao, X.; Su, L.; Wei, P.; Zhang, L.; Zhan, L.; Chong, Y.; Zhu, H.; Tsuji, N. Effect of high pressure torsion process on the microhardness, microstructure and tribological property of Ti6Al4V alloy. *J. Mater. Sci.* **2021**, *94*, 183–195. [[CrossRef](#)]
3. Souza, P.M.; Mendiguren, J.; Chao, Q.; Beladi, H.; Hodgson, P.D.; Rolfe, B.A. Microstructural based constitutive approach for simulating hot deformation of Ti6Al4V alloy in the $\alpha + \beta$ phase region. *Mater. Sci. Eng. A* **2019**, *748*, 30–37. [[CrossRef](#)]
4. Hong, J.I.A.; Fu-sheng, L.U.; Bin, H.A.O. Report on China Titanium industry progress in 2020. *Titanium Ind. Prog.* **2021**, *38*, 34–41.
5. Koizumi, H.; Takeuchi, Y.; Imai, H.; Kawai, T.; Yoneyama, T. Application of titanium and titanium alloys to fixed dental prostheses. *J. Prosthodont. Res.* **2019**, *63*, 266–270. [[CrossRef](#)] [[PubMed](#)]
6. Davim, J.P. *Machining of Titanium Alloys*; Springer: Berlin, Germany, 2014.
7. Singh, P.; Pungotra, H.; Kalsi, N.S. On the characteristics of titanium alloys for the aircraft applications—ScienceDirect. *Mater. Today Proc.* **2017**, *4*, 8971–8982. [[CrossRef](#)]
8. Yang, Y.; Zhang, C.; Dai, Y.; Luo, J. Tribological properties of titanium alloys under lubrication of SEE oil and aqueous solutions. *Tribol. Int.* **2017**, *109*, 40–47. [[CrossRef](#)]
9. Cheng, J.; Yang, J.; Ma, J.; Bi, Q.; Zhang, X.; Fu, L.; Li, F.; Zhu, S.; Liu, W. The tribological behavior of a Ti-46Al-2Cr-2Nb alloy under liquid paraffine lubrication. *Tribol. Lett.* **2012**, *46*, 233–241. [[CrossRef](#)]
10. Xie, H.; Wei, Y.; Jiang, B.; Tang, C.; Nie, C. Tribological properties of carbon nanotube/SiO₂ combinations as water-based lubricant additives for magnesium alloy. *J. Mater. Res. Technol.* **2021**, *12*, 138–149. [[CrossRef](#)]
11. Sharma, M.D.; Sehgal, R. Experimental study of friction and wear characteristics of titanium alloy (Ti-6Al-4V) under lubricated sliding condition. *Ind. Lubr. Tribol.* **2014**, *66*, 174–183. [[CrossRef](#)]
12. Wang, Q.; Hou, T.; Wang, W.; Zhang, G.; Gao, Y.; Wang, K. Tribological behavior of black phosphorus nanosheets as water-based lubrication additives. *Friction* **2022**, *10*, 374–387. [[CrossRef](#)]
13. Wang, W.; Dong, S.; Gao, Y.; Zhang, G.; Wang, K. Tribological behaviours of black phosphorus/MoS₂ composites as water-based lubrication additives. *Lubr. Sci.* **2021**, *3*, 404–416. [[CrossRef](#)]
14. Li, Z.; Ma, S.; Zhang, G.; Wang, D.; Zhou, F. Soft/Hard-Coupled Amphiphilic Polymer Nanospheres for Water Lubrication. *ACS Appl. Mater. Interfaces* **2018**, *10*, 9178–9187. [[CrossRef](#)] [[PubMed](#)]
15. Podgornik, B.; Kafexhiu, F.; Kosec, T.; Jerina, J.; Kalin, M. Friction and anti-galling properties of hexagonal boron nitride (h-BN) in aluminium forming. *Wear* **2017**, *388*, 2–8. [[CrossRef](#)]
16. Xie, G.; Luo, J.; Guo, D.; Liu, S. Nanoconfined ionic liquids under electric fields. *Appl. Phys. Lett.* **2010**, *96*, 2071. [[CrossRef](#)]
17. Xu, Y.; Nan, F.; Xu, B.S. Tribological properties of attapulgite/oil-soluble nano-Cu composite lubrication additive. *J. Mater. Eng.* **2016**, *44*, 41–46.
18. Xie, H.; Jiang, B.; Liu, B.; Wang, Q.; Xu, J.; Pan, F. An investigation on the tribological performances of the SiO₂/MoS₂ hybrid nanofluids for magnesium alloy-steel contacts. *Nanoscale Res. Lett.* **2016**, *11*, 329–346. [[CrossRef](#)]
19. Pu, J.B.; Wang, L.P.; Xue, Q.J. Progress of tribology of graphene and graphene-based composite lubrication materials. *Tribology* **2014**, *34*, 93–112.

20. Xing, C.; Zhang, J.; Jing, J.; Li, J.; Shi, F. Preparations, properties and applications of low-dimensional black phosphorus. *Chem. Eng. J.* **2019**, *370*, 120–135. [[CrossRef](#)]
21. Qu, G.; Liu, W.; Zhao, Y.; Gao, J.; Xia, T.; Shi, J.; Hu, L.; Zhou, W.; Gao, J.; Wang, H.; et al. Improved biocompatibility of black phosphorus nanosheets by chemical modification. *Angew. Chem. Int. Ed.* **2017**, *56*, 14488–14493. [[CrossRef](#)]
22. Wang, W.; Xie, G.; Luo, J. Black phosphorus as a new lubricant. *Friction* **2018**, *6*, 116–142. [[CrossRef](#)]
23. Wang, W.; Xie, G.; Luo, J. Superlubricity of Black Phosphorus as Lubricant Additive. *ACS Appl. Mater. Interfaces* **2018**, *10*, 43203–43210. [[CrossRef](#)] [[PubMed](#)]
24. Wu, S.; He, F.; Xie, G.; Bian, Z.; Luo, J.; Wen, S. Black phosphorus: Degradation favors lubrication. *Nano Lett.* **2018**, *18*, 5618–5627. [[CrossRef](#)] [[PubMed](#)]
25. Ren, X.; Yang, X.; Xie, G.; Luo, J. Black phosphorus quantum dots in aqueous ethylene glycol for macroscale superlubricity. *ACS Appl. Nano Mater.* **2020**, *3*, 4799–4809. [[CrossRef](#)]
26. Tang, W.; Jiang, Z.; Wang, B.; Li, Y. Black phosphorus quantum dots: A new-type of water-based high-efficiency lubricant additive. *Friction* **2020**, *9*, 1528–1542. [[CrossRef](#)]
27. Wu, H.; Zhao, J.; Cheng, X.; Xia, W.; He, A.; Yun, J.H.; Huang, S.; Wang, L.; Huang, H.; Jiao, S. Friction and wear characteristics of TiO₂ nano-additive water-based lubricant on ferritic stainless steel. *Tribol. Int.* **2018**, *117*, 24–38. [[CrossRef](#)]
28. Peng, D.X.; Chen, C.H.; Kang, Y.; Chang, Y.P.; Chang, S.Y. Size effects of SiO₂ nanoparticles as oil additives on tribology of lubricant. *Ind. Lubr. Tribol.* **2013**, *62*, 111–120. [[CrossRef](#)]
29. Peng, D.X.; Chen, C.H.; Kang, Y.; Chang, Y.P.; Chang, S.Y. Tribological studies of transmission oil dispersed with molybdenum disulfide and tungsten disulfide nanoparticles. *J. Tribol.* **2017**, *139*, 041301.
30. Xie, H.; Jiang, B.; He, J.; Xia, X.; Pan, F. Lubrication performance of MoS₂ and SiO₂ nanoparticles as lubricant additives in magnesium alloy-steel contacts. *Tribol. Int.* **2016**, *93*, 63–70. [[CrossRef](#)]
31. Wang, W.; Zhang, G.; Xie, G. Ultralow concentration of graphene oxide nanosheets as oil-based lubricant additives. *Appl. Surf. Sci.* **2019**, *498*, 143683. [[CrossRef](#)]
32. Rissi, E.N.; Soignard, E.; McKiernan, K.A.; Benmore, C.J.; Yarger, J.L. Pressureinduced crystallization of amorphous red phosphorus. *Solid State Commun.* **2012**, *152*, 390–394. [[CrossRef](#)]
33. Sampath, S.; Maydannik, P.; Ivanova, T.; Homola, T.; Sillanpää, M.; Nagumothu, R.; Alagan, V. Structural and morphological characterization of Al₂O₃ coated macro-porous silicon by atomic layer deposition. *Thin Solid Film.* **2016**, *616*, 628–634. [[CrossRef](#)]
34. Boonprakob, N.; Wetchakun, N.; Phanichphant, S.; Waxler, D.; Sherrell, P.; Nattestad, A.; Chen, J.; Inceesungvorn, B. Enhanced Visible-light Photocatalytic Activity of g-C₃N₄/TiO₂ Films. *J. Colloid Interface Sci.* **2014**, *417*, 402. [[CrossRef](#)]
35. Xie, H.; Dang, S.; Jiang, B.; Xiang, L.; Zhou, S.; Sheng, H.; Yang, T.; Pan, F. Tribological performances of SiO₂/graphene combinations as water-based lubricant additives for magnesium alloy rolling. *Appl. Surf. Sci.* **2019**, *475*, 847–856. [[CrossRef](#)]
36. Ni, H.; Liu, X.; Cheng, Q.D. A New Strategy for Air-Stable Black Phosphorus Reinforced PVA Nanocomposites. *J. Mater. Chem. A* **2018**, *6*, 7142–7147. [[CrossRef](#)]
37. Meng, Y.; Su, F.; Chen, Y. A novel nanomaterial of graphene oxide dotted with Ni nanoparticles produced by supercritical CO₂-assisted deposition for reducing friction and wear. *ACS Appl. Mater. Interfaces* **2015**, *7*, 11604–11612. [[CrossRef](#)] [[PubMed](#)]
38. Gong, K.; Wu, X.; Zhao, G.; Wang, X. Nanosized MoS₂ deposited on graphene as lubricant additive in polyalkylene glycol for steel/steel contact at elevated temperature. *Tribol. Int.* **2017**, *110*, 1–7.
39. Guo, D.; Li, J.; Xie, G.; Wang, Y.; Luo, J. Elastic properties of polystyrene nanospheres evaluated with atomic force microscopy: Size effect and error analysis. *Langmuir ACS J. Surf. Colloids* **2014**, *30*, 7206–7212. [[CrossRef](#)]
40. Si, L.; Guo, D.; Luo, J.; Lu, X. Monoatomic layer removal mechanism in chemical mechanical polishing process: A molecular dynamics study. *J. Appl. Phys.* **2010**, *107*, 3115. [[CrossRef](#)]
41. Hu, Y.; Wang, Y.; Wang, C.; Ye, Y.; Zhao, H.; Li, J.; Lu, X.; Mao, C.; Chen, S.; Mao, J.; et al. One-pot pyrolysis preparation of carbon dots as eco-friendly nanoadditives of water-based lubricants. *Carbon* **2019**, *152*, 511–520. [[CrossRef](#)]
42. Zhou, Y.; Qu, J. Ionic liquids as lubricant additives: A review. *ACS Appl. Mater. Interfaces* **2017**, *9*, 3209–3222. [[CrossRef](#)] [[PubMed](#)]
43. Tu, Z.; Hu, E.; Wang, B.; David, K.D.; Seeger, P.; Moneke, M.; Stengler, R.; Hu, K.; Hu, X. Tribological behaviors of Ni-modified citric acid carbon quantum dot particles as a green additive in polyethylene glycol. *Friction* **2020**, *8*, 182–197. [[CrossRef](#)]
44. Dai, W.; Kheireddin, B.; Gao, H.; Liang, H. Roles of nanoparticles in oil lubrication. *Tribol. Int.* **2016**, *102*, 88–98. [[CrossRef](#)]
45. He, C.; Yan, H.; Li, X.; Wang, X. In situ fabrication of carbon dots-based lubricants using a facile ultrasonic approach. *Green Chem.* **2019**, *21*, 2279–2285. [[CrossRef](#)]